Effects on vesicular transport pathways at the late endosome in cells with limited very long-chain fatty acids[s]

Keisuke Obara,[1] Ryo Kojima,[1] and Akio Kihara[2]

Faculty of Pharmaceutical Sciences, Hokkaido University, Kita-ku, Sapporo 060-0812, Japan

Abstract Very long-chain fatty acids (VLCFAs), fatty acids with chain-length greater than 20 carbons, possess a wide range of biological functions. However, their roles at the molecular level remain largely unknown. In the present study, we screened for multicopy suppressors that rescued temperature-sensitive growth of VLCFA-limited yeast cells, and we identified the *VPS21* gene, encoding a Rab GTPase, as such a suppressor. When the *vps21Δ* mutation was introduced into a deletion mutant of the *SUR4* gene, which encodes a VLCFA elongase, a synthetic growth defect was observed. Endosome-mediated vesicular trafficking pathways, including endocytosis and the carboxypeptidase Y (CPY) pathway, were severely impaired in *sur4Δ vps21Δ* double mutants, while the AP-3 pathway that bypasses the endosome was unaffected. In addition, the *sur4Δ* mutant also exhibited a synthetic growth defect when combined with the deletion of *VPS3*, which encodes a subunit of the class C core vacuole/endosome tethering (CORVET) complex that tethers transport vesicles to the late endosome/multivesicular body (MVB).[ILL] These results suggest that, of all the intracellular trafficking pathways, requirement of VLCFAs is especially high in the endosomal pathways.—Obara, K., R. Kojima, and A. Kihara. **Effects on vesicular transport pathways at the late endosome in cells with limited very long-chain fatty acids.** *J. Lipid Res.* 2013. **54:** 831–842.

Supplementary key words membrane traffic • multivesicular body • Rab • GTPase • yeast

Fatty acids (FAs) are components of most cellular lipids, including glycerolipids, sphingolipids, and cholesterol esters, and their metabolism is closely related to disorders such as metabolic syndrome and lifestyle-related diseases. FAs comprise carbon chains of highly diverse chain-lengths and number of double bonds, with FAs of chain-length greater than 20 carbons termed very long-chain FAs (VLCFAs). In mammals, most saturated and monounsaturated VLCFAs are components of sphingolipids and are important for skin barrier formation, neural functions, and functional maintenance of the liver (1–3). Mammalian polyunsaturated VLCFAs are used in the generation of glycerolipids and precursors of lipid mediators, which have many physiological roles in cellular processes, such as resolution of inflammation and retinal functions (3–5). In yeast, the major VLCFA is a saturated FA with a carbon chain-length of 26 (C26:0) that is found in sphingolipids but also in glycosylphosphatidylinositol (GPI) anchors (6, 7). Yeast VLCFAs function in the maintenance of nuclear envelope integrity and in the secretory pathway (8–11). Yeast mutants deficient in VLCFA synthesis are inviable (12), indicating that functions of VLCFAs cannot not be substituted for by long-chain FAs.

VLCFAs are synthesized through the elongation of long-chain FAs or shorter VLCFAs by endoplasmic reticulum (ER) membrane-embedded enzymes (13). The elongation proceeds by a four-step cycle: *i)* condensation of malonyl-CoA with acyl-CoA to produce 3-ketoacyl-CoA; *ii)* reduction of the 3-ketoacyl-CoA to 3-hydroxyacyl-CoA; *iii)* dehydration of 3-hydroxyacyl-CoA to 2,3-*trans* enoyl-CoA; and *iv)* reduction of 2,3-*trans* enoyl-CoA to an acyl-CoA that has a chain-length of two more carbons than the precursor acyl-CoA. The first condensation reaction is the rate-limiting step and in yeast is catalyzed by two redundant elongases, Fen1 and Sur4 (14). Fen1 and Sur4 determine the length of the VLCFA products. Sur4 produces C26 VLCFA, whereas Fen1 is involved in the production of C24 or shorter VLCFAs (14, 15). Yeast cells carrying deletions

for both *FEN1* and *SUR4* are inviable, yet *fen1Δ* and *sur4Δ* single mutants are viable (12).

In yeast, the sphingolipid backbone ceramide is composed of a long-chain base and an amide bond-linked VLCFA (16, 17). The addition of a polar head group to ceramide results in a complex sphingolipid. There are three classes of complex sphingolipids in yeast: inositol phosphorylceramides (IPC), mannosylinositol phosphorylceramides (MIPC), and mannosyldiinositol phosphorylceramides [M(IP)$_2$C] (16). IPCs contain phosphoinositol as a polar group and are synthesized by Aur1 (18). Mannose is added to an IPC by the redundant enzymes Csg1 and Csh1, generating a MIPC (19). An additional phosphoinositol is transferred to the MIPC by Ipt1, producing M(IP)$_2$C (20). Yeast mutant cells lacking all complex sphingolipids (*aur1Δ*) are inviable, while those lacking M(IP)$_2$Cs (*ipt1Δ*) and those lacking both MIPCs and M(IP)$_2$Cs but containing IPCs (*csg1Δ csh1Δ*) exhibit normal vegetative growth (16, 18–20).

Involvement of VLCFAs in the yeast secretory pathway has been reported. For example, cells harboring deletions in both the *SNC1* and *SNC2* genes, which encode soluble NSF attachment protein receptors (SNARE) found on secretory vesicles, exhibit a temperature-sensitive growth phenotype and a reduction in invertase secretion (11). These phenotypes were suppressed by a loss of function mutation in *SUR4* or *FEN1*, implying that VLCFAs are potentially involved in the secretory pathway (11). In addition, in *sur4Δ* cells, the plasma membrane-localized H$^+$-ATPase Pma1 is mistargeted to the vacuole (8), and an interruption in the transcription of *PHS1*, which encodes the 3-hydroxyacyl-CoA dehydratase that catalyzes the third step of the VLCFA elongation cycle, results in impaired accumulation of mature Gas1, a GPI-anchored protein localized in the plasma membrane (9). Thus, involvement of VLCFAs in secretory pathways is now recognized. However, no report has clearly demonstrated involvement of VLCFAs in the vesicular trafficking pathway that functions in transport toward the vacuole. This is probably due to difficulties in assessing their importance under VLCFA-null, lethal conditions, in which any indirect effects could not be excluded. Thus, investigation of VLCFA function under mild conditions is required for more understanding.

In the study presented here, we carried out a genetic screen to identify genes involved in VLCFA functions. We identified the Rab GTPase *VPS21* as a multicopy suppressor of a yeast mutant with limited VLCFA synthesis. Analyses of a *sur4Δ vps21Δ* double mutant suggested that VLCFAs are involved in Vps21-related vesicular transport processes. Furthermore, the gene *SUR4* exhibited interactions with genes encoding the class C core vacuole/endosome tethering (CORVET) subunits that function in tethering of vesicles to the late endosome/multivesicular body (MVB). Considering that any yeast mutant unable to synthesize VLCFA is nonviable, VLCFAs must be important for several essential cellular processes, such as general vesicular transport. However, transport defects at the endosome appeared even under the mild, VLCFA-limited conditions used here, suggesting that the requirement for VLCFAs is especially high in the endosomal trafficking pathways.

MATERIALS AND METHODS

Yeast strains and media

The *Saccharomyces cerevisiae* strains used in this study are listed in **Table 1**. Cells were grown in YPD medium (1% yeast extract, 2% peptone, and 2% D-glucose) or in synthetic dextrose (SD) medium (0.67% yeast nitrogen base without amino acids and 2% D-glucose) supplemented with 0.5% casamino acid and appropriate supplements. Single-deletion mutants, except MRY106 (*vps19Δ::LEU2*), were purchased from Open Biosystems (Huntsville, AL). Gene disruption was performed by replacing the entirety or part of the coding region with a marker gene.

Screening of multicopy suppressors

MRY9 (*P$_{tetO7}$-PHS1 sur4Δ*) cells were transfected with a yeast genomic library, in which genomic DNAs were cloned into the yeast expression vector pRS426 (2 μ, *URA3* marker) (21). A pool of approximately 30,000 Ura$^+$ clones were plated on YPD plates and incubated for 4 days at 39°C. Plasmids were prepared from the 16 clones obtained and were reintroduced into MRY9. Of the 16 plasmids, 2 reproducibly restored growth of MRY9 at 39°C. Sequences of the DNA fragments inserted into the two plasmids were determined using a 3130 Genetic Analyzer (Applied Biosystems, Foster City, CA). Sequencing revealed that one plasmid contained the *SUR4* gene, and the other (pMR22) contained the *VPS21* and *YVC1* genes and the asparagine tRNA gene *tN(GUU) O2*. The pMR31 (*VPS21*) and pMR30 [*YVC1* and *tN(GUU)O2*] plasmids were created by subcloning the respective genes from the pMR22 plasmid into the pRS426 vector.

Plasmid construction

The pOK489 (*mRFP-CPS1*) and pOK529 (*STE2-mRFP*) plasmids were constructed as follows. The *CPS1* gene was amplified by PCR from BY4741 genomic DNA to have *Eco*RI and *Xho*I sites at the 5′ and 3′ ends, respectively. The amplified fragment was cloned into the *Eco*RI-*Xho*I site of the pOK107 plasmid (22), which contains the mRFP-2xFYVE domain, to replace the 2xFYVE domain with the *CPS1* gene, thereby producing the pOK489 plasmid. The promoter and coding region, without the stop codon, of the *STE2* gene was amplified by PCR from BY4741 genomic DNA to have *Sac*I and *Bam*HI sites at the 5′ and 3′ ends, respectively. The mRFP sequence was amplified by PCR from pOK107 so that *Bam*HI and *Xho*I sites were generated at the 5′ and 3′ ends, respectively. These fragments were cloned together into the *Sac*I-*Xho*I site of the p416TEF plasmid (23), creating the pOK529 plasmid.

The pMR8 (*FEN1*) and pMR10 (*SUR4*) plasmids were constructed as follows. The promoter, coding region, and 3′-UTR of these genes were amplified by PCR with creation of *Bam*HI site at the 5′ end. The amplified fragments of *FEN1* and *SUR4* were first cloned into the pGEM-T Easy vector (Promega, Madison, WI), then *Bam*HI-*Not*I fragments of the resulting plasmids were transferred to the yeast expression vector pRS316 (*CEN*, *URA3* marker) (24), producing the pMR8 and pMR10 plasmids.

FA elongation assays

In vitro FA elongation assays were performed essentially as described previously (25). Typical reaction mixtures contained total

TABLE 1. Yeast strains used in this study

Strain	Genotype	Source
BY4741	*MATa his3Δ1 leu2Δ0 met15Δ0 ura3Δ0*	(46)
YOK2230	BY4741, P_{tetO7}-PHS1::NatNT2 ura3Δ::MET15	This study
MRY7	BY4741, *fen1Δ::KanMX4 P_{tetO7}-PHS1::NatNT2 ura3Δ::MET15*	This study
MRY9	BY4741, *sur4Δ::KanMX4 P_{tetO7}-PHS1::NatNT2 ura3Δ::MET15*	This study
MRY90	BY4741, *vps21Δ::NatNT2 fen1Δ::KanMX4*	This study
MRY91	BY4741, *vps21 Δ::NatNT2 sur4 Δ::KanMX4*	This study
MRY106	BY4741, *vps19 Δ::LEU2*	This study
MRY121	BY4741, *vps3Δ::KanMX4 sur4Δ::NatNT2*	This study
MRY124	BY4741, *vps19Δ::LEU2 sur4Δ::NatNT2*	This study
MRY129	BY4741, *csg1Δ::natNT2 csh1Δ::LEU2*	This study
MRY134	BY4741, *ipt1Δ::KanMX4 vps21Δ::NatNT2*	This study
MRY135	BY4741, *vps8Δ::KanMX4 sur4Δ::NatNT2*	This study
MRY136	BY4741, *vps39Δ::KanMX4 sur4Δ::NatNT2*	This study
MRY137	BY4741, *vps41Δ::KanMX4 sur4Δ::NatNT2*	This study
MRY157	BY4741, *vps21Δ::NatNT2 csg1Δ::KanMX4*	This study
MRY159	BY4741, *vps21Δ::NatNT2 csh1Δ::KanMX4*	This study
MRY160	BY4741, *vps21Δ::NatNT2 csg1Δ::KanMX4 csh1Δ::LEU2*	This study
MRY235	BY4741, *vps8Δ::KanMX4 vps19Δ::LEU2*	This study
MRY242	BY4741, *vps8Δ::KanMX4 vps19Δ::LEU2 sur4Δ::NatNT2*	This study
405	BY4741, *vps8Δ::KanMX4*	(47)
1865	BY4741, *vps21Δ::KanMX4*	(47)
2771	BY4741, *csg1Δ::KanMX4*	(47)
3300	BY4741, *csh1Δ::KanMX4*	(47)
3774	BY4741, *vps39Δ::KanMX4*	(47)
4007	BY4741, *ipt1Δ::KanMX4*	(47)
4015	BY4741, *vps41Δ::KanMX4*	(47)
4329	BY4741, *vps3Δ::KanMX4*	(47)
5281	BY4741, *sur4Δ::KanMX4*	(47)
5763	BY4741, *fen1Δ::KanMX4*	(47)

membrane fractions (20 μg protein), 20 μM palmitoyl-CoA complexed with 0.2 mg/ml FA-free BSA (Sigma, St. Louis, MO), 73 μM malonyl-CoA, and 27.3 μM [^{14}C]malonyl-CoA (0.075 μCi; Moravek Biochemicals, Brea, CA) in a 50 μl reaction mixture. After the reaction, lipids were saponified, acidified, extracted, and dried as described previously (25). FAs were then converted to methyl esters by dissolving in 67 μl of 3 M methanolic-HCl (final 1 M), 123 μl of chloroform, and 10 μl of 2,2-dimethoxypropane (final concentration 5%), and incubating at 100°C for 1 h. Samples were then treated with 233 μl methanol, 177 μl chloroform, and 300 μl of 1% (w/v) KCl with vigorous mixing, and the organic phase was recovered and dried. Lipids were suspended in 20 μl chloroform and separated by reverse-phase TLC on LKC18 Silica Gel 60 TLC plates (Whatman, Kent, UK) with chloroform/methanol/water (5:15:1, v/v) as the solvent system. Labeled lipids were detected by autoradiography.

Immunoblotting

Total cell lysates were prepared by the alkaline/trichloroacetic acid method as described previously (22). Proteins were separated by SDS-PAGE and transferred to Immobilon polyvinylidene difluoride membrane (Millipore, Billerica, MA). The membrane was incubated with an anti-DsRed (1:1000 dilution; a kind gift from Dr. S. Nishikawa), anti-CPY (0.25 μg/ml; Molecular Probes, Eugene, OR), anti-Pep4 (1:5000 dilution; a kind gift from Dr. Y. Ohsumi), anti-ALP (1:5000 dilution; a kind gift from Dr. Y. Ohsumi), or anti-Pgk1 (0.25 μg/ml; Molecular Probes) antibody, and then with HRP-conjugated anti-rabbit or anti-mouse IgG F(ab′)$_2$ fragment (1:10,000 dilution; GE Healthcare Bio-Sciences, Piscataway, NJ). Signals were detected using an ECL prime (GE Healthcare Bio-Sciences) or Western Lightning Plus-ECL (Perkin-Elmer Life Sciences, Waltham, MA) kit and an ImageQuant LAS 4000 Biomolecular Imager (Fuji Photo Film, Tokyo, Japan). The Pep4 signal was enhanced using Can Get Signal Immunoreaction Enhancer Solution (TOYOBO, Osaka, Japan).

Pulse-chase experiment

Cells were grown at 30°C in SD medium containing appropriate supplements but lacking methionine and cysteine. Cells (2.0 A_{600} units) were pulse-labeled with 100 μCi [^{35}S]methionine/cysteine (EasyTag EXPRE^{35}S^{35}S Protein Labeling Mix; PerkinElmer Life Sciences) at 30°C for 15 min. Chase was initiated upon addition of unlabeled methionine and cysteine to a final concentration of 5 mM and 1 mM, respectively. The reaction was terminated by addition of sodium azide to a final concentration of 20 mM, and cells were kept on ice. Cells were collected by centrifugation, suspended in lysis buffer [50 mM Tris-HCl (pH 6.8), 2% SDS, 10% glycerol, and 1% 2-mercaptoethanol], broken by vigorously mixing with glass beads, and boiled for 3 min. Then the resulting lysates (30 μl) were diluted with 1 ml Triton buffer [50 mM Tris-HCl (pH 8.0), 150 mM NaCl, 0.1 mM EDTA (pH 8.0), and 2% Triton X-100]. After removal of insoluble materials by centrifugation, samples were incubated with 750 ng of anti-CPY antibody (Molecular Probes) and 15 μl of Protein G-Sepharose (GE Healthcare Bio-Sciences) for 16 h at 4°C with rotation. After beads were washed once with Triton buffer and once with Wash buffer [10 mM Tris-HCl (pH 8.0) and 150 mM NaCl], bound proteins were eluted with 2× SDS sample buffer [100 mM Tris-HCl, (pH 6.8), 4% SDS, 20% glycerol, 12% 2-mercaptoethanol, and a trace amount of bromophenol blue] and subjected to SDS-PAGE. The gel was fixed with 10% acetic acid and 20% methanol, treated with Amplify fluorographic reagent (GE Healthcare Bio-Sciences), and detected using a bioimaging analyzer BAS-2500 (Fuji Photo Film).

Microscopy

Cells were cultured to log phase in SD medium supplemented with 0.5% casamino acid and appropriate supplements and observed under a fluorescence microscope (Axioimager M2, Carl Zeiss, Oberkochen, Germany).

RESULTS

Yeast cells' requirement of VLCFAs for growth is significant at elevated temperature

To begin to understand the functions of VLCFA in yeast, we first examined their roles in growth using a mutant with reduced VLCFA synthesis. Complete abrogation of VLCFA synthesis, such as that resulting from a double deletion of the redundant elongases *FEN1* and *SUR4*, is lethal (12), so we first examined the growth of *fen1Δ* and *sur4Δ* single-mutant cells at high temperature. Both mutants exhibited normal growth at 30°C; however, at 39°C the growth of the *sur4Δ* cells was retarded compared with the growth of wild-type cells (**Fig. 1A**). This phenotype was enhanced by decreasing the levels of the 3-hydroxyacyl-CoA dehydratase Phs1, which is involved in the third step of the VLCFA elongation cycle, using genetic manipulation. Replacement of the *PHS1* promoter with the doxycycline-dependent *tetO*$_7$ promoter (P_{tetO7}) reduces the Phs1 levels to approximately 1/20 of normal even in the absence of doxycycline treatment (26). P_{tetO7}-*PHS1 sur4Δ* cells could not grow at 39°C at all (Fig. 1A). P_{tetO7}-*PHS1 fen1Δ* cells also exhibited a severe growth defect at 39°C. These results indicate that the cells' requirement for VLCFAs is particularly significant at high temperatures.
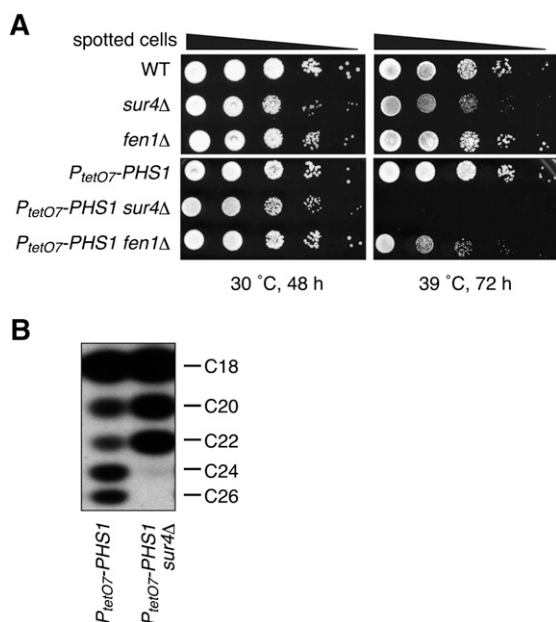

Fig. 1. Cells' requirement of VLCFA is significant at elevated temperature. (A) BY4741 (wild-type), 5281 (*sur4Δ*), 5763 (*fen1Δ*), YOK2230 (P_{tetO7}-*PHS1*), MRY9 (P_{tetO7}-*PHS1 sur4Δ*), and MRY7 (P_{tetO7}-*PHS1 fen1Δ*) cells were grown to stationary phase, serially diluted at 1:10, spotted on YPD plates, grown for the indicated times at 30°C or 39°C, and photographed against a dark background. (B) YOK2230 (P_{tetO7}-*PHS1*) and MRY9 (P_{tetO7}-*PHS1 sur4Δ*) cells were grown to log phase at 30°C, and total membrane fractions were prepared. Samples (20 μg) were incubated with 20 μM palmitoyl-CoA, 73 μM malonyl-CoA, and 27.3 μM [^{14}C]malonyl-CoA (0.075 μCi) for 1 h at 37°C. Lipids were saponified, acidified, extracted, converted to methyl ester forms, separated by reverse-phase TLC, and detected by autoradiography.

To reveal any relationship between the chain-length of the VLCFAs and the growth requirement observed above, we examined the elongase activity of the P_{tetO7}-*PHS1 sur4Δ* cells in vitro using palmitoyl-CoA as a substrate. The P_{tetO7}-*PHS1* cells were able to elongate palmitoyl-CoA to C26-CoA, but in the P_{tetO7}-*PHS1 sur4Δ* cells elongation beyond C22-CoA was largely impaired, with no C26-CoA and only small amounts of C24-CoA produced (Fig. 1B). These results suggest that VLCFAs with a chain-length of 26 and/or 24 carbons are required for cell growth at 39°C.

Overexpression of *VPS21* suppresses the temperature sensitivity of the VLCFA-limited cells

To identify genes that exhibit a close relationship with VLCFA function, we employed a multicopy suppressor screening. P_{tetO7}-*PHS1 sur4Δ* cells were transfected with a yeast genomic DNA library, and suppressors that restored growth at 39°C were isolated. Of two suppressors we obtained, one comprised a plasmid containing the *SUR4* gene. The other suppressor harbored a plasmid containing a genomic region encompassing the *VPS21* gene, which encodes a Rab-type small GTPase involved in vesicular trafficking to the vacuole (27, 28) (supplementary Fig. I-A). Further subcloning and growth suppression assays determined that the *VPS21* gene indeed functions as a multicopy suppressor in P_{tetO7}-*PHS1 sur4Δ* cells at high temperatures (supplementary Fig. I-B). To clarify whether overexpression of Vps21 restored growth by facilitating synthesis of C24 and/or C26 VLCFA, we performed a VLCFA elongation assay. Expression of Sur4 restored the VLCFA elongation activity that produces C26-CoA and that was defective in the P_{tetO7}-*PHS1 sur4Δ* cells, but no significant difference was observed in the VLCFA elongation activity of P_{tetO7}-*PHS1 sur4Δ* cells overexpressing Vps21 and those harboring an empty vector (supplementary Fig. I-C). Thus, Vps21 does not regulate VLCFA synthesis but may be related to the cellular functions in which VLCFAs are involved.

Deletion of the *VPS21* gene causes a synthetic growth defect with deletion of the elongase genes

The growth defect in cells grown at 39°C was observed not only for P_{tetO7}-*PHS1 sur4Δ* cells but also for *sur4Δ* cells, albeit to a lesser extent (Fig. 1A). For simplification, we used the *sur4Δ* cells for further analyses. The *sur4Δ* cells exhibited only slight growth retardation, both at 30°C and 36°C (**Fig. 2A**). Growth of the *vps21Δ* cells was only slightly retarded at 36°C, although a significant growth defect was observed at 39°C (Fig. 2A), as reported for 38°C (28). When a *vps21Δ* mutation was introduced into the *sur4Δ* cells, the resulting *sur4Δ vps21Δ* cells exhibited more severe growth retardation at 30°C than would be expected as an additive effect of the two single mutations (Fig. 2A), indicating a synthetic growth defect. Furthermore, we even observed a synthetic lethal phenotype at 36°C (Fig. 2A). A *fen1Δ vps21Δ* double mutant also displayed a synthetic growth defect both at 30°C and 36°C (Fig. 2A). To address whether the synthetic effects observed were the result of alterations in VLCFA synthesis, we performed FA elongation assays. The wild-type membrane elongated C16-CoA up to C26-CoA
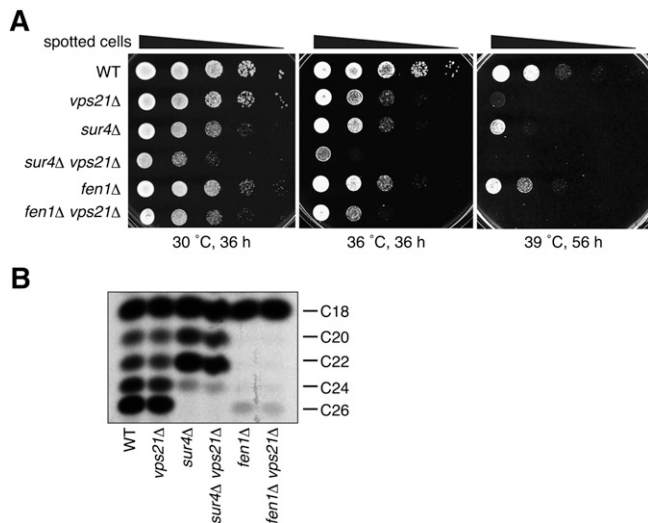
Fig. 2. Deletion of the *SUR4* and *VPS21* genes results in synthetic growth defect. (A) BY4741 (wild-type), 1865 (*vps21Δ*), 5281 (*sur4Δ*), MRY91 (*sur4Δ vps21Δ*), 5763 (*fen1Δ*), and MRY90 (*fen1Δ vps21Δ*) cells were grown to stationary phase, serially diluted at 1:10, spotted on YPD plates, grown for indicated time at 30°C, 36°C, or 39°C, and photographed against a dark background. (B) Total membrane fractions (20 μg) prepared from BY4741 (wild-type), 1865 (*vps21Δ*), 5281 (*sur4Δ*), MRY91 (*sur4Δ vps21Δ*), 5763 (*fen1Δ*), and MRY90 (*fen1Δ vps21Δ*) cells grown at 30°C were incubated with 20 μM palmitoyl-CoA, 73 μM malonyl-CoA, and 27.3 μM [^{14}C]malonyl-CoA (0.075 μCi) for 1 h at 37°C. Lipids were saponified, acidified, extracted, converted to methyl ester forms, separated by reverse-phase TLC, and detected by autoradiography.

(Fig. 2B). However, elongations beyond C18-CoA and C22-CoA were largely impaired in *fen1Δ* and *sur4Δ* cells, respectively. These results were consistent with the previous lipidomic analysis (6), in which C16/C18 and C22 sphingolipids were increased in *fen1Δ* and *sur4Δ* cells, respectively.

Sphingolipid synthesis is known to be affected by the *sur4Δ* or *fen1Δ* mutation (6, 14). However, introducing the *vps21Δ* mutation into the *sur4Δ* or *fen1Δ* mutant had no further effect on sphingolipid synthesis as judged by [^{14}C] serine or [^{3}H]dihydrosphingosine labeling (supplementary Fig. II-A, B). Thus, Vps21 is not involved in the regulation of VLCFA or sphingolipid synthesis, but it may be related to the functions of VLCFAs.

Pathways governing protein transport toward the vacuole via the late endosome/MVB are impaired in *sur4Δ vps21Δ* and *fen1Δ vps21Δ* mutants

The genetic interactions between *VPS21* and *SUR4/FEN1* observed above suggest that VLCFAs have roles in pathways involved in vesicular transport toward the vacuole via the endosome, in which Vps21 is involved. Thus, we monitored vesicular transport to the vacuole in *sur4Δ vps21Δ* and *fen1Δ vps21Δ* cells. To avoid potential secondary effects caused by the lethality of *sur4Δ vps21Δ* mutations at 36°C, we examined the vesicular transport at 30°C. The soluble vacuolar proteases carboxypeptidase Y (CPY) and Pep4 are synthesized in the ER and delivered to the vacuole via the Golgi apparatus and the late endosome/MVB, a pathway called the CPY pathway. Immunoblots revealed

that substantial levels of CPY were present intracellularly as the mature, vacuole form in wild-type, *fen1Δ*, and *sur4Δ* cells (**Fig. 3A**). In *vps21Δ* cells, the mature CPY was also apparent, but its levels were decreased compared with those in wild-type cells, and small amounts of the p2 (Golgi) form were observed intracellularly. The reduction in intracellular CPY was due to missorting of the p2 CPY to the extracellular space (Fig. 3A), as others have reported (27, 29). In contrast, *sur4Δ vps21Δ* and *fen1Δ vps21Δ* cells accumulated significant levels of the p1 (ER) and p2 (Golgi) forms of CPY, in addition to the mature form, indicating that the CPY pathway was affected synthetically by these double mutations (Fig. 3A). Secretion of the p2 form was also observed in both *sur4Δ vps21Δ* and *fen1Δ vps21Δ* cells, suggesting that the late secretory pathways are not impaired in these cells. Such synthetic effects were also confirmed by a pulse-chase experiment (Fig. 3B). Nearly all newly synthesized CPY was converted to the mature
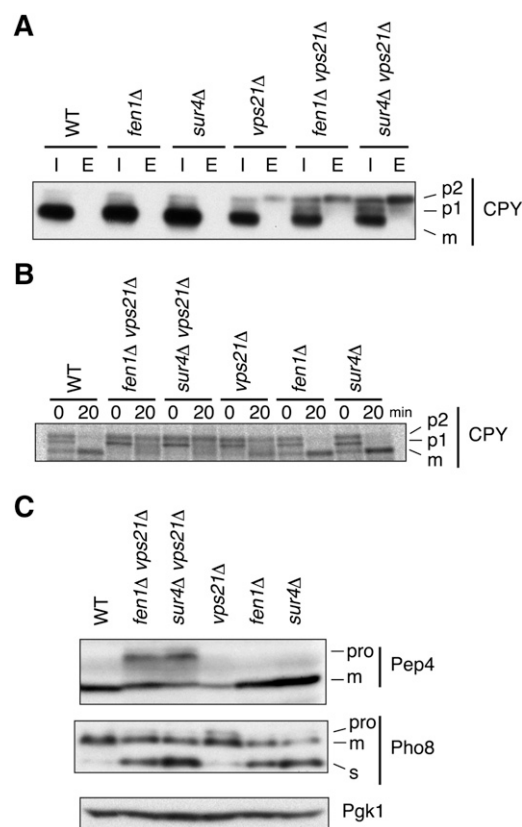

Fig. 3. The CPY pathway is affected in *sur4Δ vps21Δ* and *fen1Δ vps21Δ* mutants. BY4741 (wild-type), MRY90 (*fen1Δ vps21Δ*), MRY91 (*sur4Δ vps21Δ*), 1865 (*vps21Δ*), 5763 (*fen1Δ*), and 5281 (*sur4Δ*) cells were grown at 30°C to log phase. (A) Intracellular total lysates (I) and extracellular proteins recovered from the medium (E) were separated by SDS-PAGE, followed by immunoblotting with an anti-CPY antibody. (B) Cells were pulse-labeled with 100 μCi [^{35}S]methionine/cysteine for 15 min and chased for 20 min. Total lysates were prepared, and CPY was immunoprecipitated with an anti-CPY antibody. Precipitates were subjected to SDS-PAGE and detected using a bioimaging analyzer BAS-2500. (C) Total lysates were prepared, separated by SDS-PAGE, and detected by immunoblotting with an anti-Pep4, anti-Pho8, or to demonstrate uniform protein loading, anti-Pgk1 antibody. m, mature form; pro, proform; s, soluble mature form.

form within 20 min in wild-type, *fen1Δ*, and *sur4Δ* cells. In *vps21Δ* cells, though, the mature CPY levels were decreased compared with those in wild-type cells, and significant amounts of the p2 form were detected after a 20 min chase. Introducing the *fen1Δ* or *sur4Δ* mutation into the *vps21Δ* cells enhanced the defect in the CPY transport. The mature CPY was nearly undetectable after a 20 min chase, and the p2 levels became more prominent in these double mutants (Fig. 3B). Similar results were obtained for Pep4. Nearly all Pep4 was detected as the mature form in wild-type, *vps21Δ*, *fen1Δ*, and *sur4Δ* cells, whereas in *vps21Δ* cells the Pep4 levels were decreased (Fig. 3C). In contrast, *sur4Δ vps21Δ* and *fen1Δ vps21Δ* cells significantly accumulated the Pep4 proform. These results indicate that the deletions of *VPS21* and *SUR4* or *FEN1* synthetically affect the CPY pathway.

We next examined the transport of the vacuolar carboxypeptidase Cps1. Cps1 is synthesized as a membrane protein in the ER, then transported to the vacuole lumen via the Golgi and the late endosome/MVB, where it is sorted into the intraluminal vesicles, then processed to its mature form. Fluorescence microscopy using mRFP-fused Cps1 (mRFP-Cps1) indicated that Cps1 was normally localized in the vacuole lumen in wild-type cells (**Fig. 4A**). In *sur4Δ* and *fen1Δ* cells, vacuoles were highly fragmented, as reported by others (30, 31) (Fig. 4A and supplementary Fig. III). Fluorescence of mRFP was detected in the fragmented vacuoles, indicating that mRFP-Cps1 did reach the vacuole lumen in these mutants (Fig. 4A and supplementary Fig. IV). In *vps21Δ* cells, mRFP-Cps1 was detected mainly in the vacuole lumen. In addition, some mRFP-Cps1 signals were detected at the vacuole membrane and as intracellular punctuates (Fig. 4A), indicating that mRFP-Cps1 transport was slightly retarded in the *vps21Δ* cells. In the *sur4Δ vps21Δ* and *fen1Δ vps21Δ* mutants, mRFP-Cps1 transport to the vacuole was severely impaired. Almost no mRFP-Cps1 was observed in the vacuole lumen, but mRFP-Cps1 accumulated on the vacuolar membranes, in a perivacuolar compartment, probably representing MVB, and in some punctate structures in the cytosol (Fig. 4A and supplementary Fig. IV). Interestingly, fragmentation of the vacuole observed in the *sur4Δ* and *fen1Δ* mutants was reduced in these double mutants (supplementary Fig. III).

We also confirmed the defect in Cps1 transport in *sur4Δ vps21Δ* and *fen1Δ vps21Δ* cells by immunoblot using an anti-DsRed antibody that detects mRFP. After delivery into the vacuole lumen, the linker portion of mRFP-Cps1 is cleaved by vacuolar proteases, releasing the mRFP moiety (32). The free mRFP was detected in wild-type, *vps21Δ*, *fen1Δ*, and *sur4Δ* cells but not in *sur4Δ vps21Δ* or *fen1Δ vps21Δ* cells (Fig. 4B), indicating that mRFP-Cps1 was not delivered to the vacuole lumen in the *sur4Δ vps21Δ* or *fen1Δ vps21Δ* cells. These results indicate that the transport of membrane proteins via intraluminal vesicle formation is severely impaired in *sur4Δ vps21Δ* and *fen1Δ vps21Δ* cells.

We next investigated the endocytic pathway in *sur4Δ vps21Δ* and *fen1Δ vps21Δ* cells using Ste2, a G protein-coupled receptor for a mating pheromone (33), as a marker protein. Plasma membrane-localized Ste2 is internalized
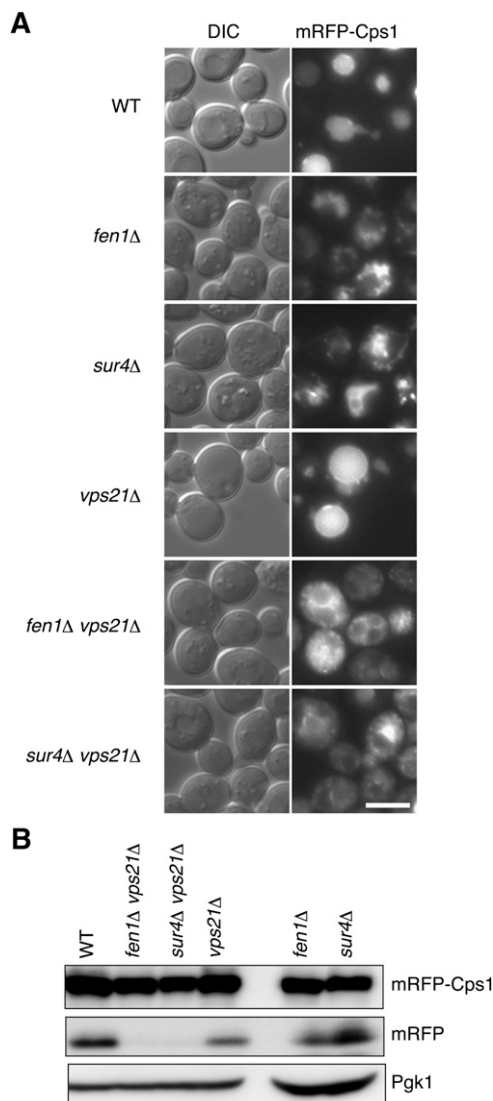

Fig. 4. Transport of Cps1 to the vacuole is impaired in *sur4Δ vps21Δ* and *fen1Δ vps21Δ* mutants. (A) BY4741 (wild-type), 5763 (*fen1Δ*), 5281 (*sur4Δ*), 1865 (*vps21Δ*), MRY90 (*fen1Δ vps21Δ*), and MRY91 (*sur4Δ vps21Δ*) cells, each harboring pOK489 (mRFP-Cps1), were grown at 30°C to log phase and subjected to fluorescence microscopy. Left panels, DIC images; right panels, mRFP fluorescence. Bar, 5 μm. (B) Total lysates were prepared from cells indicated in (A), separated by SDS-PAGE, and detected by immunoblotting with anti-DsRed antibody or, to demonstrate uniform protein loading, anti-Pgk1 antibody. Expression levels of mRFP-Cps1 were significantly low in the *fen1Δ* and *sur4Δ* mutants, compared with the other strains used, for an unknown reason. Thus, the amounts of lysates subjected to SDS-PAGE were increased for the *fen1Δ* and *sur4Δ* mutants (3- and 4-fold for the *fen1Δ* and *sur4Δ* cells, respectively) to make the total amount of mRFP-Cps1 plus mRFP comparable to the other strains.

into the cell by endocytosis and delivered to the vacuole via the late endosome/MVB (34, 35). In wild-type cells, the fluorescence of Ste2-mRFP was mainly detected in the vacuole lumen (**Fig. 5A** and supplementary Fig. V). The endocytic pathway was also not significantly affected in *sur4Δ* or *fen1Δ* cells, since Ste2-mRFP was observed in the lumen of the fragmented vacuoles (Fig. 5A and supplementary Fig. V). In *vps21Δ* cells, Ste2-mRFP was detected
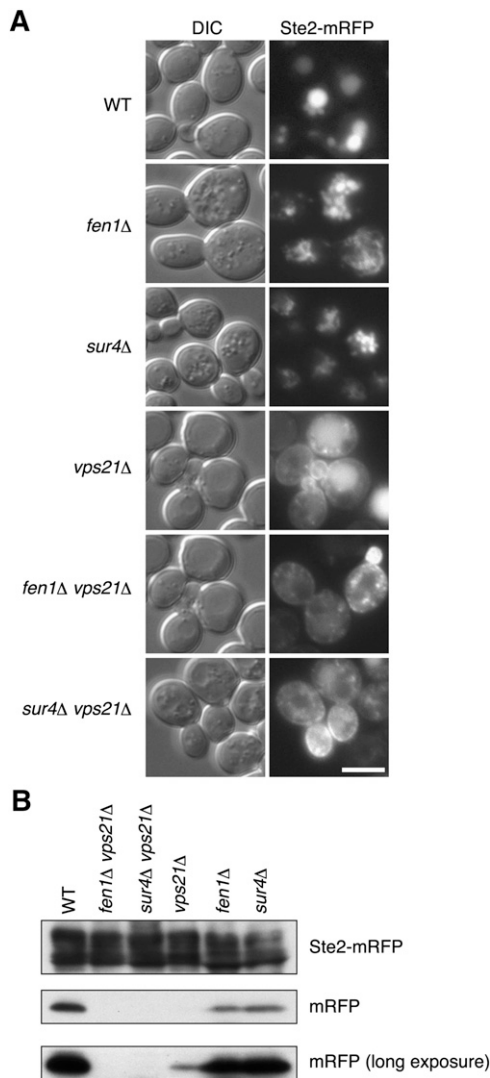
Fig. 5. Endocytosis of Ste2 is impaired in *sur4Δ vps21Δ* and *fen1Δ vps21Δ* cells. (A) BY4741 (wild-type), 5763 (*fen1Δ*), 5281 (*sur4Δ*), 1865 (*vps21Δ*), MRY90 (*fen1Δ vps21Δ*), and MRY91 (*sur4Δ vps21Δ*) cells, each harboring pOK529 (Ste2-mRFP), were grown at 30°C to log phase and subjected to fluorescence microscopy. Left panels, DIC images; right panels, mRFP fluorescence. Bar, 5 μm. (B) Total lysates were prepared from cells indicated in (A) and separated by SDS-PAGE, followed by immunoblotting with anti-DsRed antibody or, to demonstrate uniform protein loading, anti-Pgk1 antibody. The lower panel represents the same immunoblot as the middle panel but a longer exposure to X-ray film performed to enhance the image.

at the plasma membrane and as intracellular punctuates, as well as in the vacuole lumen, indicating that endocytosis of Ste2-mRFP is severely affected in the *vps21Δ* cells, consistent with reports that Vps21 is involved in endocytosis (36). In the *sur4Δ vps21Δ* and *fen1Δ vps21Δ* double mutants, the Ste2-mRFP signal was mainly detected at the plasma membrane and in some punctate structures in the cytosol (Fig. 5A and supplementary Fig. V). However, it was not clear whether the endocytotic pathways in the *sur4 Δ vps21Δ* and *fen1Δ vps21Δ* double mutants were more severely affected than those in the *vps21Δ* cells from these fluorescence microscopic results. Therefore, we also evaluated

Ste2-mRFP endocytosis by immunoblot. In strong agreement with the results of the microscopy, the mRFP moiety released from Ste2-mRFP in the vacuole was detected in wild-type, *fen1Δ*, and *sur4Δ* cells (Fig. 5B). Free mRFP was largely reduced in *vps21Δ* cells but could still be detected (Fig. 5B). However, no free mRFP was detected in *sur4Δ vps21Δ* or *fen1Δ vps21Δ* cells (Fig. 5B). Thus, similar to results with the Cps1 transport, synthetic effects of *vps21Δ* and *sur4Δ* or *fen1Δ* were observed in Ste2-mRFP endocytosis.

Some vacuolar proteins are transported to the vacuole directly from the Golgi without passing through the late endosome/MVB. This pathway is called the AP-3 pathway. The alkaline phosphatase Pho8, a type II membrane protein, is the most characterized cargo of this pathway (37, 38). The 74 kDa Pho8 proform is processed into a 72 kDa mature form upon delivery to the vacuoles, and some protein is further processed into a 66 kDa soluble mature form (39). In wild-type cells, most of the Pho8 detected was the mature form, and almost no proform was observed (Fig. 3C). In contrast, in *vps21Δ* cells, a fraction of the Pho8 was present as the proform, as reported by others (40). In *sur4Δ* and *fen1Δ* cells, almost all of the Pho8 was the vacuole form, either the mature or soluble mature form (Fig. 3C), suggesting that the AP-3 pathway was not impaired. The soluble mature form was increased in the *sur4Δ* and *fen1Δ* cells compared with wild-type cells due to some unknown reason. Introduction of the *vps21Δ* mutation into the *sur4Δ* or *fen1Δ* cells had no effect on the maturation of Pho8 (Fig. 3C), suggesting that the AP-3 pathway was intact in the *sur4Δ vps21Δ* and *fen1Δ vps21Δ* cells. Overall, protein transport pathways utilizing the late endosome/MVB were impaired in the *sur4Δ vps21Δ* and *fen1Δ vps21Δ* cells, but those pathways that bypass the organelle were not.

Sphingolipids containing VLCFAs function in Vps21-related vesicular transport pathways

In yeast, the vast majority of VLCFAs are incorporated into sphingolipids as part of the hydrophobic backbone formed by ceramide, which contains FA such as a VLCFA (16, 17). Thus, it is highly likely that VLCFAs acting in Vps21-involved trafficking events function as components of sphingolipids. Each sphingolipid also comprises a polar head group on the ceramide. We considered the polar head groups of sphingolipids and investigated their roles in Vps21-related vesicular transport pathways. Although *aur1Δ* cells, which lack all complex sphingolipids including IPC, MIPC, and M(IP)$_2$C, are not able to grow in culture, yeast cells that lack only M(IP)$_2$C (*ipt1Δ* cells) and those that lack MIPC and M(IP)$_2$C (*csg1Δ csh1Δ* cells) are able to grow without any retardation under normal vegetative conditions. We introduced the *ipt1Δ* mutation or *csg1Δ csh1Δ* double-deletion mutation into *vps21Δ* cells and examined the effect on cell growth and on the vesicular transports of the CPY and AP-3 pathways, as well as Cps1 transport and endocytosis.

Growth of the *ipt1Δ vps21Δ* cells at 30°C and 36°C was comparable to that of wild-type cells or those carrying either single mutation (**Fig. 6A**). Likewise, the *csg1Δ csh1Δ*

mutants grew normally, whereas in contrast, the *csg1Δ csh1Δ vps21Δ* triple mutant displayed severe growth defects, especially at 36°C (Fig. 6B). To further analyze the synthetic effect of the *csg1Δ csh1Δ* and *vps21Δ* mutations, vesicular transport pathways in the *csg1Δ csh1Δ vps21Δ* cells were compared with those in the *csg1Δ csh1Δ* and *vps21Δ* cells. To avoid potential secondary effects caused by the severe growth defect of the *csg1Δ csh1Δ vps21Δ* mutations observed at 36°C, we examined the vesicular transport at 30°C. Fluorescence microscopy indicated that mRFP-Cps1 transport was impaired in *csg1Δ csh1Δ vps21Δ* cells so that mRFP-Cps1 rarely reached the vacuole lumen and instead accumulated at the vacuolar membrane, late endosome/MVB, and intracellular punctate structures (Fig. 6C and supplementary Fig. IV). In immunoblots, free mRFP was detected in the wild-type and *csg1Δ csh1Δ* cells and also in the *vps21Δ* cells, albeit at a reduced level (Fig. 6D). On the other hand, little free mRFP was observed in the *csg1Δ csh1Δ vps21Δ* cells (Fig. 6D), confirming that

transport of mRFP-Cps1 to the vacuole was impaired. Furthermore, impairments were observed in CPY and Pep4 transport (Fig. 6D) and in endocytosis of Ste2-mRFP (Fig. 6C and supplementary Fig. V) in the *csg1Δ csh1Δ vps21Δ* cells. Similar to results in *sur4Δ vps21Δ* cells, delivery of Pho8 to the vacuole via the AP-3 pathway was not affected in the *csg1Δ csh1Δ vps21Δ* cells (Fig. 6D). These findings suggest that sphingolipids are indeed involved in Vps21-related vesicular transport at the late endosome/MVB. As the *csg1Δ csh1Δ* mutation and the *sur4Δ* mutation affect mannose and VLCFA moieties of sphingolipids, respectively, both moieties are important in this transport.

SUR4 genetically interacts with genes encoding subunits of the CORVET complex

It is known that Vps21 physically interacts with the CORVET complex, which is involved in membrane tethering at the late endosome/MVB (41). Thus, interactions between *SUR4* and genes encoding the CORVET subunits
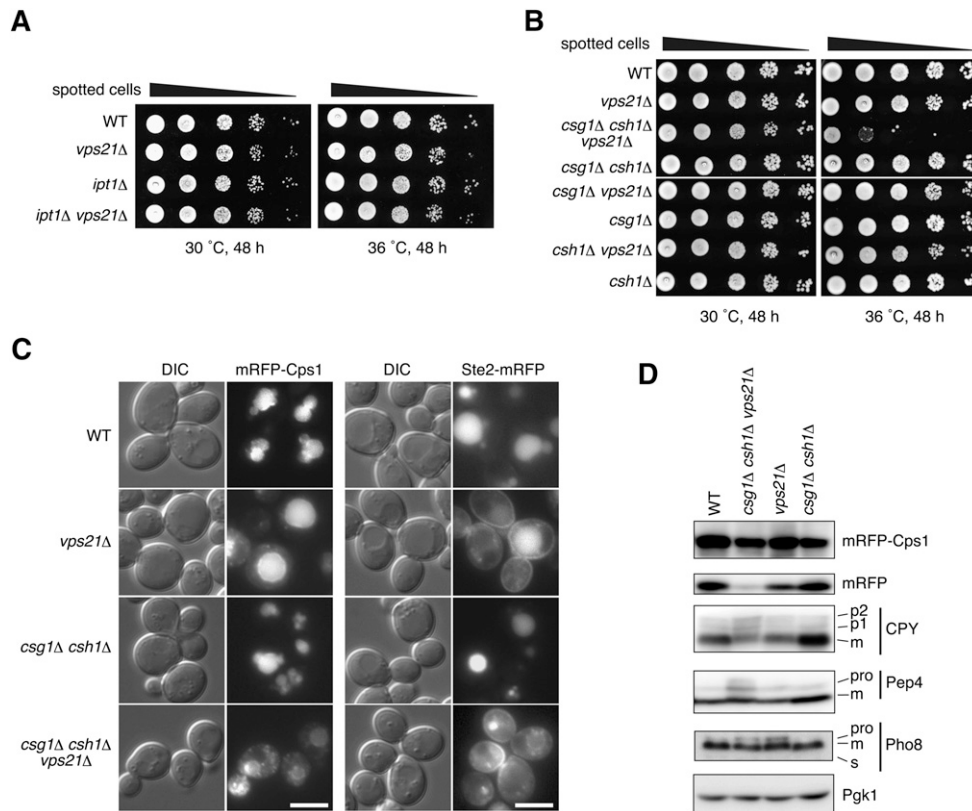

Fig. 6. Sphingolipids containing VLCFAs cooperate with Vps21 in vesicular transport pathways that traffic to the vacuole. (A) BY4741 (wild-type), 1865 (*vps21Δ*), 4007 (*ipt1Δ*), and MRY134 (*ipt1Δ vps21Δ*) cells were grown to stationary phase, serially diluted at 1:10, spotted on YPD plates, grown for 48 h at 30°C or 36°C, and photographed against a dark background. (B) BY4741 (wild-type), 1865 (*vps21Δ*), MRY160 (*csg1Δ csh1Δ vps21Δ*), MRY129 (*csg1Δ csh1Δ*), MRY157 (*csg1Δ vps21Δ*), 2771 (*csg1Δ*), MRY159 (*csh1Δ vps21Δ*), and 3300 (*csh1Δ*) cells were grown to stationary phase, serially diluted at 1:10, spotted on YPD plates, grown for 48 h at 30°C or 36°C, and photographed against a dark background. (C) BY4741 (wild-type), 1865 (*vps21Δ*), MRY129 (*csg1Δ csh1Δ*), and MRY160 (*csg1Δ csh1Δ vps21Δ*) cells, each harboring pOK489 (mRFP-Cps1) or pOK529 (Ste2-mRFP), were grown at 30°C to log phase, then subjected to fluorescence microscopy. Left panels, DIC images; right panels, mRFP fluorescence. Bars, 5 μm. (D) BY4741 (wild-type), MRY160 (*csg1Δ csh1Δ vps21Δ*), 1865 (*vps21Δ*), and MRY129 (*csg1Δ csh1Δ*) cells, alone or transfected with pOK489 (mRFP-Cps1), were grown at 30°C to log phase. Total lysates were extracted and separated by SDS-PAGE, and proteins were detected by immunoblotting with an anti-DsRed, anti-CPY, anti-Pep4, anti-Pho8, or to demonstrate uniform protein loading, anti-Pgk1 antibody. m, mature form; pro, proform.

were examined at the genetic level. The CORVET complex is composed of six subunits. Vps3 and Vps8 are specific to the CORVET complex, whereas four other subunits, Vps11, Vps16, Vps18, and Vps33, are shared with the homotypic fusion and vacuole protein sorting (HOPS) complex, which is involved in membrane tethering at the vacuole (**Fig. 7C**) (42). The HOPS complex also contains Vps39 and Vps41 as specific subunits in place of Vps3 and Vps8. The factors that are specific to the CORVET and HOPS complexes are interchangeable, and thus mixed complexes (i-CORVET containing Vps3 and Vps41, and i-HOPS containing Vps39 and Vps8) also exist (41). Severe synthetic growth defect at 36°C was observed in cells carrying a deletion of the *SUR4* gene together with a deletion of *VPS3* (Fig. 7A). Deletion of *VPS8*, another gene encoding a CORVET-specific subunit, the Vps21 effector, conferred a synthetic growth defect at 36°C when combined with the *SUR4* deletion (Fig. 7A), although the effect was weaker than that observed with the *VPS3* deletion. This weak phenotype may be explained by the functional complementation of another Vps21 effector, Vps19 (43), as simultaneous deletion of *VPS19* and *VPS8* in *sur4*Δ cells caused a severe synthetic growth defect at nearly the same levels as found in the *sur4*Δ *vps21*Δ and *sur4*Δ *vps3*Δ mutants (Fig. 7B). In addition, deletion of *VPS41* or *VPS39*, which encode

HOPS-specific components, caused a moderate synthetic growth defect at 36°C when combined with the *SUR4* deletion, implying that i-CORVET and i-HOPS formation affects the levels, function, or stability of the CORVET complex. These results further reinforce the notion that VLCFAs function in vesicular trafficking at the late endosome/MVB together with Vps21.

DISCUSSION

VLCFAs have essential physiological functions in eukaryotes, and cells carrying double deletions of the redundant yeast FA elongases *FEN1* and *SUR4*, which are involved in VLCFA synthesis, cannot grow in any temperature (12). However, it still remains unclear in which cellular processes VLCFAs exert their essential functions. In the presented study using yeast cells that produce limited VLCFAs, we found that the VLCFA requirement is especially high at elevated temperatures. On the basis of this finding, we carried out a genetic screening to identify factors that are related to VLCFA functions at the molecular level, and we identified the *VPS21* gene as an important player in these processes. Subsequent genetic and cell biological analyses suggest that VLCFAs are involved in the vesicular transport
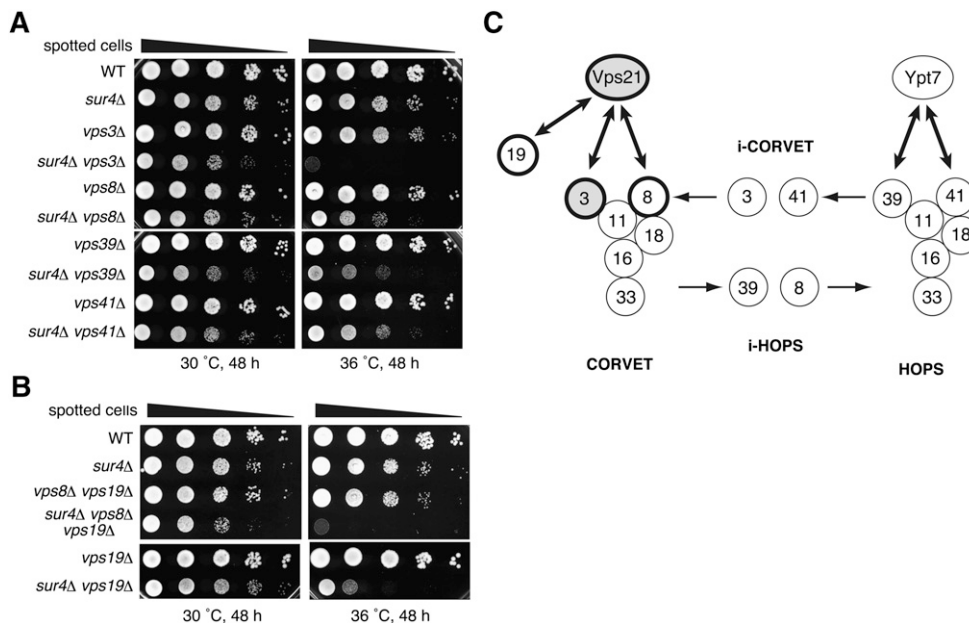

Fig. 7. The *SUR4* gene interacts at the genetic level with genes encoding CORVET subunits. (A) BY4741 (wild-type), 5281 (*sur4*Δ), 4329 (*vps3*Δ), MRY121 (*sur4*Δ *vps3*Δ), 405 (*vps8*Δ), MRY135 (*sur4*Δ *vps8*Δ), 3774 (*vps39*Δ), MRY136 (*sur4*Δ *vps39*Δ), 4015 (*vps41*Δ), and MRY137 (*sur4*Δ *vps41*Δ) cells were grown to stationary phase, serially diluted at 1:10, spotted on YPD plates, grown for 48 h at 30°C or 36°C, and photographed against a dark background. (B) BY4741 (wild-type), 5281 (*sur4*Δ), MRY235 (*vps8*Δ *vps19*Δ), MRY242 (*sur4*Δ *vps8*Δ *vps19*Δ), MRY106 (*vps19*Δ), and MRY124 (*sur4*Δ *vps19*Δ) cells were grown to stationary phase, serially diluted at 1:10, spotted on YPD plates, grown for 48 h at 30°C or 36°C, and photographed against a dark background. (C) Schematic representation of the CORVET and HOPS complexes and interactions between their encoding genes and the *SUR4* gene. Deletion of *VPS21* or *VPS3* causes severe synthetic growth defect when combined with the *SUR4* deletion; these genes are illustrated as filled gray circles with thick lines. Simultaneous disruption of genes encoding the Vps21 effectors *VPS8* and *VPS19* also results in severe synthetic growth defect when combined with the *SUR4* deletion; these genes are illustrated as white circles enclosed by thick lines. Two-headed arrows indicate protein-protein interactions between Rab GTPases and proteins involved in vesicle tethering.

pathways that act at the late endosome/MVB. Although VLCFAs have been implicated in the secretory pathway, our research provides the first experimental evidence that VLCFAs are also involved in endosomal trafficking.

The most severe synthetic growth defect was observed in *sur4Δ vps21Δ* or *sur4Δ vps3Δ* cells (Figs. 2A and 7A). Vps3 is a specific component of the CORVET complex, which captures the vesicle at the late endosome/MVB by physically interacting with Vps21 (41). Simultaneous deletion of the two Vps21 effectors (*VPS19* and *VPS8*) in *sur4Δ* cells also caused a very severe synthetic growth defect (Fig. 7B). Thus, all the mutations that lead to loss of Vps21 function caused the severe synthetic growth defect when combined with *sur4Δ* mutation. Since genetic interactions have been observed between genes functioning in closely related cellular processes in general, we speculate that Vps21 cooperates with VLCFAs in vesicle fusions with the late endosome/MVB. Alternatively or in addition, both Vps21-mediated vesicle fusion with the late endosome/MVB and the function of VLCFAs in the late endosome/MVB may be highly important for the functional maintenance of this organelle.

Then what is the function of VLCFA in vesicular trafficking, especially at the late endosome/MVB? During vesicle budding and fusion, local generation of highly curved membranes is essential, for example, at the neck of budding vesicles and at the contact sites of lipid mixing during vesicle fusion. The chain-length of VLCFAs allows them to span both leaflets of the lipid bilayer, which would facilitate generation and stabilization of highly curved membranes. Such membrane-stabilizing functions of VLCFAs have been proposed for the formation of the nuclear pore complex, around which highly curved membranes also exist (10). Thus, it would seem likely that VLCFAs are involved in vesicular trafficking by stabilizing highly curved membranes. Similar to conditions observed for vesicle budding and fusion, intraluminal vesicle formation at the late endosome/MVB requires generation of highly curved membrane at the neck of invagination. We detected mRFP-Cps1 on the vacuole membrane in the *sur4Δ vps21Δ* and *fen1Δ vps21Δ* mutants (Fig. 4A), suggesting that VLCFAs are also required for the formation of intraluminal vesicles. Such frequent generation of curved membranes at the late endosome/MVB may cause this organelle to be highly sensitive to VLCFA-limited conditions. In the present study, we found that the VLCFA requirement is significant at elevated temperatures (Fig. 1A). It is possible that curved membrane structures are destabilized at elevated temperatures due to enhanced membrane fluidity, leading to a high VLCFA requirement.

In yeast, almost no free VLCFAs exist, and most VLCFAs are incorporated into sphingolipids, although small amounts are used for GPI-anchor generation. Since GPI-anchored proteins are localized in the plasma membrane and are not involved in vesicular transport at the late endosome/MVB, the functions of VLCFAs revealed here must be elicited by those VLCFAs that are components of sphingolipids. Indeed, *csg1Δ csh1Δ vps21Δ* triple-mutant cells, which are defective in MIPC synthesis, exhibited a growth defect at a high temperature and impairment in vesicular transport

pathways active at the late endosome/MVB (Fig. 6). This further indicates that not only the VLCFA moiety but also the polar head group of a sphingolipid is important for Vps21-related membrane fusion. Although the *csg1Δ csh1Δ vps21Δ* cells possess IPCs, the simplest complex sphingolipids, they do not have mannose-containing MIPCs or M(IP)$_2$Cs. We speculate that mannose facilitates clustering of sphingolipids through hydrogen bonds and stabilizes the membrane curvature generated by VLCFAs.

It is known that vacuoles in *sur4Δ* and *fen1Δ* mutants are fragmented (30, 31), which we confirmed in this study (Figs. 4 and 5 and supplementary Fig. III). Interestingly, though, fragmentation of the vacuole was diminished in *sur4Δ vps21Δ* and *fen1Δ vps21Δ* cells. Cells carrying deletions for *VPS21* possess a single enlarged vacuole and are known as having a class D *vps* phenotype (29). Hence, in regards to their vacuole morphology, *sur4Δ vps21Δ* and *fen1Δ vps21Δ* mutants exhibited an intermediate phenotype compared with each single mutant. This counteractive effect on vacuole morphology is in contrast to the synergetic effects observed here for cell growth at high temperature and vesicular transport. Thus, the mechanisms may differ for the effects of VLCFAs on vacuole morphology and on vesicular transport pathways active at the late endosome/MVB. Vacuole fragmentation is often accompanied by defects in vacuolar protein maturation and transport (44, 45). However, neither *sur4Δ* cells nor *fen1Δ* cells exhibited significant defects in transport of vacuolar proteins into their fragmented vacuoles (Figs. 3 and 4). Interestingly, levels of the soluble mature form of Pho8, a highly processed form of the mature protein, were increased in *sur4Δ*, *fen1Δ*, *sur4Δ vps21Δ*, and *fen1Δ vps21Δ* cells (Fig. 3C), although the mechanism behind this enhanced processing is not readily understood. This phenomenon was not tightly coupled with vacuole fragmentation, as the *sur4Δ vps21Δ* and *fen1Δ vps21Δ* double mutants, in which vacuole fragmentation was less prominent, also accumulated the soluble mature Pho8 at levels similar to those in the *sur4Δ* and *fen1Δ* single mutants. In addition, unlike the defects in the endosome-mediated transport pathways, this phenomenon was not enhanced synergetically by the combination of *VPS21* deletion and deletion of *SUR4* or *FEN1*. Thus, this phenomenon was associated with the deletion of *SUR4* or *FEN1* but not with *VPS21* deletion. Indeed, the soluble mature Pho8 was undetectable in the *csg1Δ csh1Δ vps21Δ* triple mutant.

In the presented study, we revealed the function of VLCFAs in vesicular transport at the late endosome/MVB. However, considering that VLCFAs are essential for cell growth, it is highly likely that VLCFAs function in several membrane-involved processes, including other vesicular transport pathways, as reported for the secretory pathway. Indeed, we observed an accumulation of the p1 ER form of CPY in *fen1Δ vps21Δ* and *sur4Δ vps21Δ* cells, even under our mild conditions (Fig. 3A), suggesting that vesicular transport from the ER to the Golgi is also affected. Currently, the specific process(es) in which VLCFAs are actually involved, such as vesicle budding or fusion of the vesicle with the destination membrane, remains unclear.

Dissection of the vesicular transport pathway into its elementary processes and an assessment of VLCFA functions in each will be needed for further understanding.⬛

REFERENCES

1. Mizutani, Y., S. Mitsutake, K. Tsuji, A. Kihara, and Y. Igarashi. 2009. Ceramide biosynthesis in keratinocyte and its role in skin function. *Biochimie.* **91:** 784–790.

2. Imgrund, S., D. Hartmann, H. Farwanah, M. Eckhardt, R. Sandhoff, J. Degen, V. Gieselmann, K. Sandhoff, and K. Willecke. 2009. Adult ceramide synthase 2 (CERS2)-deficient mice exhibit myelin sheath defects, cerebellar degeneration and hepatocarcinomas. *J. Biol. Chem.* **284:** 33549–33560.

3. Kihara, A. 2012. Very long-chain fatty acids: elongation, physiology and related disorders. *J. Biochem.* **152:** 387–395.

4. Bannenberg, G., and C. N. Serhan. 2010. Specialized pro-resolving lipid mediators in the inflammatory response: an update. *Biochim. Biophys. Acta.* **1801:** 1260–1273.

5. Agbaga, M. P., M. N. Mandal, and R. E. Anderson. 2010. Retinal very long-chain PUFAs: new insights from studies on ELOVL4 protein. *J. Lipid Res.* **51:** 1624–1642.

6. Ejsing, C. S., J. L. Sampaio, V. Surendranath, E. Duchoslav, K. Ekroos, R. W. Klemm, K. Simons, and A. Shevchenko. 2009. Global analysis of the yeast lipidome by quantitative shotgun mass spectrometry. *Proc. Natl. Acad. Sci. USA.* **106:** 2136–2141.

7. Fujita, M., and Y. Jigami. 2008. Lipid remodeling of GPI-anchored proteins and its function. *Biochim. Biophys. Acta.* **1780:** 410–420.

8. Gaigg, B., B. Timischl, L. Corbino, and R. Schneiter. 2005. Synthesis of sphingolipids with very long chain fatty acids but not ergosterol is required for routing of newly synthesized plasma membrane ATPase to the cell surface of yeast. *J. Biol. Chem.* **280:** 22515–22522.

9. Yu, L., L. Pena Castillo, S. Mnaimneh, T. R. Hughes, and G. W. Brown. 2006. A survey of essential gene function in the yeast cell division cycle. *Mol. Biol. Cell.* **17:** 4736–4747.

10. Schneiter, R., M. Hitomi, A. S. Ivessa, E. V. Fasch, S. D. Kohlwein, and A. M. Tartakoff. 1996. A yeast acetyl coenzyme A carboxylase mutant links very-long-chain fatty acid synthesis to the structure and function of the nuclear membrane-pore complex. *Mol. Cell. Biol.* **16:** 7161–7172.

11. David, D., S. Sundarababu, and J. E. Gerst. 1998. Involvement of long chain fatty acid elongation in the trafficking of secretory vesicles in yeast. *J. Cell Biol.* **143:** 1167–1182.

12. Revardel, E., M. Bonneau, P. Durrens, and M. Aigle. 1995. Characterization of a new gene family developing pleiotropic phenotypes upon mutation in *Saccharomyces cerevisiae. Biochim. Biophys. Acta.* **1263:** 261–265.

13. Jakobsson, A., R. Westerberg, and A. Jacobsson. 2006. Fatty acid elongases in mammals: their regulation and roles in metabolism. *Prog. Lipid Res.* **45:** 237–249.

14. Oh, C. S., D. A. Toke, S. Mandala, and C. E. Martin. 1997. *ELO2* and *ELO3,* homologues of the *Saccharomyces cerevisiae ELO1* gene, function in fatty acid elongation and are required for sphingolipid formation. *J. Biol. Chem.* **272:** 17376–17384.

15. Denic, V., and J. S. Weissman. 2007. A molecular caliper mechanism for determining very long-chain fatty acid length. *Cell.* **130:** 663–677.

16. Dickson, R. C., C. Sumanasekera, and R. L. Lester. 2006. Functions and metabolism of sphingolipids in *Saccharomyces cerevisiae. Prog. Lipid Res.* **45:** 447–465.

17. Kihara, A., S. Mitsutake, Y. Mizutani, and Y. Igarashi. 2007. Metabolism and biological functions of two phosphorylated sphingolipids, sphingosine 1-phosphate and ceramide 1-phosphate. *Prog. Lipid Res.* **46:** 126–144.

18. Nagiec, M. M., E. E. Nagiec, J. A. Baltisberger, G. B. Wells, R. L. Lester, and R. C. Dickson. 1997. Sphingolipid synthesis as a target for antifungal drugs. Complementation of the inositol phosphorylceramide synthase defect in a mutant strain of *Saccharomyces cerevisiae* by the *AUR1* gene. *J. Biol. Chem.* **272:** 9809–9817.

19. Uemura, S., A. Kihara, J. Inokuchi, and Y. Igarashi. 2003. Csg1p and newly identified Csh1p function in mannosylinositol phosphorylceramide synthesis by interacting with Csg2p. *J. Biol. Chem.* **278:** 45049–45055.

20. Dickson, R. C., E. E. Nagiec, G. B. Wells, M. M. Nagiec, and R. L. Lester. 1997. Synthesis of mannose-(inositol-P)2-ceramide, the major sphingolipid in *Saccharomyces cerevisiae,* requires the *IPT1* (*YDR072c*) gene. *J. Biol. Chem.* **272:** 29620–29625.

21. Kihara, A., and Y. Igarashi. 2002. Identification and characterization of a *Saccharomyces cerevisiae* gene, *RSB1,* involved in sphingoid long-chain base release. *J. Biol. Chem.* **277:** 30048–30054.

22. Obara, K., T. Noda, K. Niimi, and Y. Ohsumi. 2008. Transport of phosphatidylinositol 3-phosphate into the vacuole via autophagic membranes in *Saccharomyces cerevisiae. Genes Cells.* **13:** 537–547.

23. Mumberg, D., R. Muller, and M. Funk. 1995. Yeast vectors for the controlled expression of heterologous proteins in different genetic backgrounds. *Gene.* **156:** 119–122.

24. Sikorski, R. S., and P. Hieter. 1989. A system of shuttle vectors and yeast host strains designed for efficient manipulation of DNA in *Saccharomyces cerevisiae. Genetics.* **122:** 19–27.

25. Ohno, Y., S. Suto, M. Yamanaka, Y. Mizutani, S. Mitsutake, Y. Igarashi, T. Sassa, and A. Kihara. 2010. ELOVL1 production of C24 acyl-CoAs is linked to C24 sphingolipid synthesis. *Proc. Natl. Acad. Sci. USA.* **107:** 18439–18444.

26. Kihara, A., H. Sakuraba, M. Ikeda, A. Denpoh, and Y. Igarashi. 2008. Membrane topology and essential amino acid residues of Phs1, a 3-hydroxyacyl-CoA dehydratase involved in very long-chain fatty acid elongation. *J. Biol. Chem.* **283:** 11199–11209.

27. Robinson, J. S., D. J. Klionsky, L. M. Banta, and S. D. Emr. 1988. Protein sorting in *Saccharomyces cerevisiae:* isolation of mutants defective in the delivery and processing of multiple vacuolar hydrolases. *Mol. Cell. Biol.* **8:** 4936–4948.

28. Horazdovsky, B. F., G. R. Busch, and S. D. Emr. 1994. *VPS21* encodes a rab5-like GTP binding protein that is required for the sorting of yeast vacuolar proteins. *EMBO J.* **13:** 1297–1309.

29. Raymond, C. K., I. Howald-Stevenson, C. A. Vater, and T. H. Stevens. 1992. Morphological classification of the yeast vacuolar protein sorting mutants: evidence for a prevacuolar compartment in class E vps mutants. *Mol. Biol. Cell.* **3:** 1389–1402.

30. Kohlwein, S. D., S. Eder, C. S. Oh, C. E. Martin, K. Gable, D. Bacikova, and T. Dunn. 2001. Tsc13p is required for fatty acid elongation and localizes to a novel structure at the nuclear-vacuolar interface in *Saccharomyces cerevisiae. Mol. Cell. Biol.* **21:** 109–125.

31. Chung, J. H., R. L. Lester, and R. C. Dickson. 2003. Sphingolipid requirement for generation of a functional V_1 component of the vacuolar ATPase. *J. Biol. Chem.* **278:** 28872–28881.

32. Suzuki, K., Y. Kamada, and Y. Ohsumi. 2002. Studies of cargo delivery to the vacuole mediated by autophagosomes in *Saccharomyces cerevisiae. Dev. Cell.* **3:** 815–824.

33. Burkholder, A. C., and L. H. Hartwell. 1985. The yeast alpha-factor receptor: structural properties deduced from the sequence of the *STE2* gene. *Nucleic Acids Res.* **13:** 8463–8475.

34. Konopka, J. B., D. D. Jenness, and L. H. Hartwell. 1988. The C-terminus of the S. cerevisiae α-pheromone receptor mediates an adaptive response to pheromone. *Cell.* **54:** 609–620.

35. Reneke, J. E., K. J. Blumer, W. E. Courchesne, and J. Thorner. 1988. The carboxy-terminal segment of the yeast alpha-factor receptor is a regulatory domain. *Cell.* **55:** 221–234.

36. Gerrard, S. R., N. J. Bryant, and T. H. Stevens. 2000. *VPS21* controls entry of endocytosed and biosynthetic proteins into the yeast prevacuolar compartment. *Mol. Biol. Cell.* **11:** 613–626.

37. Cowles, C. R., G. Odorizzi, G. S. Payne, and S. D. Emr. 1997. The AP-3 adaptor complex is essential for cargo-selective transport to the yeast vacuole. *Cell.* **91:** 109–118.

38. Stepp, J. D., K. Huang, and S. K. Lemmon. 1997. The yeast adaptor protein complex, AP-3, is essential for the efficient delivery of alkaline phosphatase by the alternate pathway to the vacuole. *J. Cell Biol.* **139:** 1761–1774.

39. Klionsky, D. J., and S. D. Emr. 1989. Membrane protein sorting: biosynthesis, transport and processing of yeast vacuolar alkaline phosphatase. *EMBO J.* **8:** 2241–2250.

40. Anand, V. C., L. Daboussi, T. C. Lorenz, and G. S. Payne. 2009. Genome-wide analysis of AP-3-dependent protein transport in yeast. *Mol. Biol. Cell.* **20:** 1592–1604.

41. Peplowska, K., D. F. Markgraf, C. W. Ostrowicz, G. Bange, and C. Ungermann. 2007. The CORVET tethering complex interacts with the yeast Rab5 homolog Vps21 and is involved in endo-lysosomal biogenesis. *Dev. Cell.* **12:** 739–750.

42. Bowers, K., and T. H. Stevens. 2005. Protein transport from the late Golgi to the vacuole in the yeast *Saccharomyces cerevisiae. Biochim. Biophys. Acta.* **1744:** 438–454.

43. Tall, G. G., H. Hama, D. B. DeWald, and B. F. Horazdovsky. 1999. The phosphatidylinositol 3-phosphate binding protein Vac1p interacts with a Rab GTPase and a Sec1p homologue to facilitate vesicle-mediated vacuolar protein sorting. *Mol. Biol. Cell.* **10:** 1873–1889.

44. Wada, Y., Y. Ohsumi, and Y. Anraku. 1992. Genes for directing vacuolar morphogenesis in *Saccharomyces cerevisiae*. I. Isolation and characterization of two classes of vam mutants. *J. Biol. Chem.* **267:** 18665–18670.

45. Sato, T. K., T. Darsow, and S. D. Emr. 1998. Vam7p, a SNAP-25-like molecule, and Vam3p, a syntaxin homolog, function together in yeast vacuolar protein trafficking. *Mol. Cell. Biol.* **18:** 5308–5319.

46. Brachmann, C. B., A. Davies, G. J. Cost, E. Caputo, J. Li, P. Hieter, and J. D. Boeke. 1998. Designer deletion strains derived from *Saccharomyces cerevisiae* S288C: a useful set of strains and plasmids for PCR-mediated gene disruption and other applications. *Yeast.* **14:** 115–132.

47. Winzeler, E. A., D. D. Shoemaker, A. Astromoff, H. Liang, K. Anderson, B. Andre, R. Bangham, R. Benito, J. D. Boeke, H. Bussey, et al. 1999. Functional characterization of the *S. cerevisiae* genome by gene deletion and parallel analysis. *Science.* **285:** 901–906.